nature climate change

LETTERS

PUBLISHED ONLINE: 18 MAY 2015 | DOI: 10.1038/NCLIMATE2646

# Trade-off between intensity and frequency of global tropical cyclones

Nam-Young Kang[1,2]* and James B. Elsner[1]

**Global tropical cyclone climate has been investigated with indicators of frequency, intensity[1] and activity[2,3]. However, a full understanding of global warming's influence on tropical cyclone climate remains elusive because of the incomplete nature of these indicators. Here we form a complete three-dimensional variability space of tropical cyclone climate where the variabilities are continuously linked and find that global ocean warmth best explains the out-of-phase relationship between intensity and frequency of global tropical cyclones. In a year with greater ocean warmth, the tropical troposphere is capped by higher pressure anomaly in the middle and upper troposphere even with higher moist static energy anomaly in the lower troposphere, which is thought to inhibit overall tropical cyclone occurrences but lead to greater intensities. A statistical consequence is the trade-off between intensity and frequency. We calculate an average increase in global tropical cyclone intensity of 1.3 m s$^{-1}$ over the past 30 years of ocean warming occurring at the expense of 6.1 tropical cyclones worldwide.**

Tropical cyclones (TCs) are perhaps the least welcomed natural phenomena on our planet. Even well-developed and highly complex societies are vulnerable to their destructiveness because of significant exposure[4,5]. Ocean warmth is increasing with global warming and a major concern is how TC climate will change. Recent studies from theoretical and numerical projections of future TC climate reveal decreasing frequency and increasing intensity in this warming environment[6,7]. Nevertheless, there is little observational support, except for the increasing intensity of the strongest portion of TCs (refs 8,9). Trend analysis is a popular approach, but results are constrained by a focus on just a few TC climate indicators (for example, accumulated cyclone energy). Is it possible that the influence of global warming on TCs is aligned somewhere in between these indicators?

Here we examine a globally consistent TC response to ocean warming by linearly linking frequency, intensity and activity in a continuous variability space[10]. The linear approach is expected to provide a convenient framework for understanding the TC climate structure. TCs whose lifetime-maximum wind (LMW) speed exceeds 17 m s$^{-1}$ are selected annually. In this framework, the annual number of TC occurrences and the annual mean LMW are used as indicators for frequency ($F$) and intensity ($I$), respectively. These two primary TC indicators are not orthogonal to each other, but the corresponding eigenvectors derived from a principal component analysis create a continuous TC variability space (Supplementary Fig. 1). The principal component of the in-phase relationship between $F$ and $I$ indicates a variability direction close to those of the accumulated cyclone energy (ACE) and power dissipation index (PDI; Supplementary Fig. 6). This variability direction is named $A$ to stand for 'activity', and note the other principal component indicates a variability direction orthogonal to $A$. This variability represents the out-of-phase relationship between $F$ and $I$, and is named $E$ to stand for 'efficiency of intensity', as it shows how much more $I$ contributes to $A$ than does $F$. Practically, $E$ reveals the degree of trade-off between $I$ and $F$ at a given $A$. If it were not for $E$, the TC climate variability space with $I$, $F$ and $A$ would not span the two-dimensional variability space.

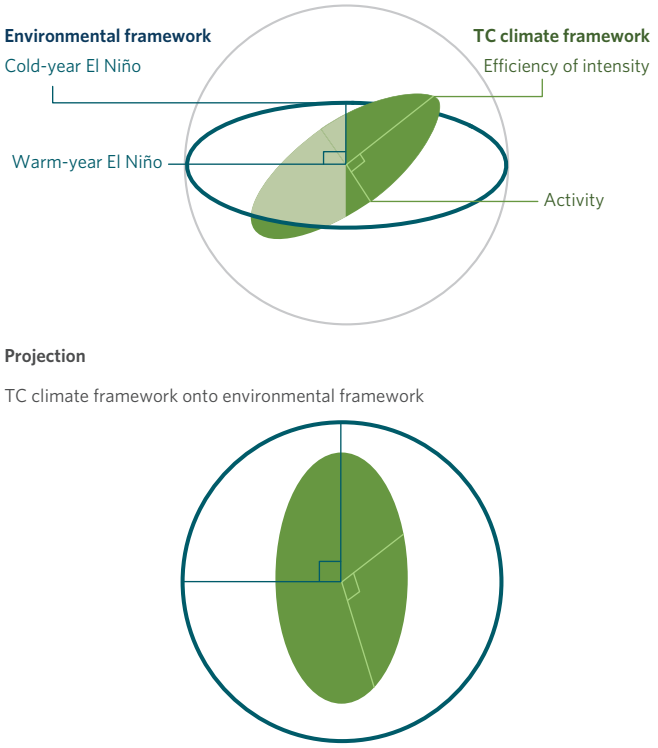


**Figure 1 | Schematic of a three-dimensional variability space.** The TC climate variability space and the environmental variability space are constructed separately. The two variability spaces have a crossing angle and different magnitudes. The projection of TC climate onto the environmental climate shows which environmental variable best explains each TC climate variability direction.

The same orthogonal structure is applied to our environmental framework, where the Southern Oscillation Index (SOI) and global sea surface temperature (SST) are chosen as the primary indicators (Supplementary Fig. 3). The former indicates El Niño ($N$) and the latter global ocean warmth ($O$). This environmental space suggests two orthogonal variabilities of warm-year El Niño ($W$) and cold-year El Niño ($C$), which are indicated by the two principal

[1]Florida State University, Tallahassee, Florida 32306, USA. [2]Korea Meteorological Administration, Seoul 156720, South Korea. *e-mail: nkang@fsu.edu

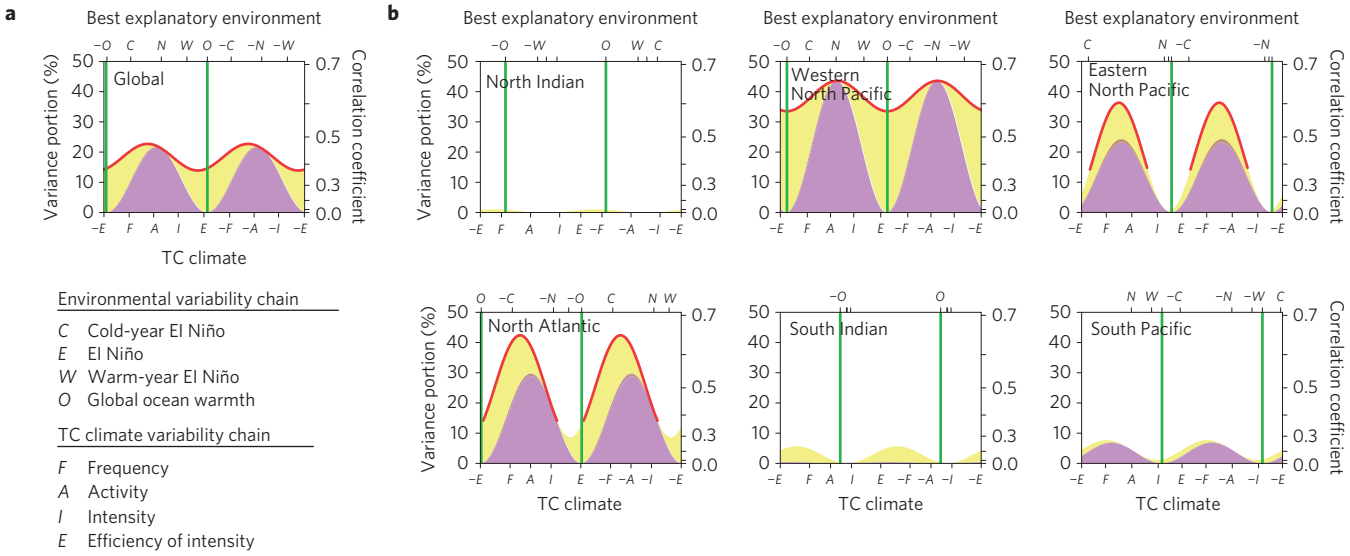


**Figure 2 | Projection length of TC climate framework onto environmental framework. a**, Projected length of global TC climate variabilities. **b**, Projected length of six regional TC climate variabilities. The length represents the correlation coefficient. Variance portion (%) shows how much the best explanatory environment (upper abscissa) explains each TC climate variability (lower abscissa). Significance of the correlation coefficient is examined using *t*-values. The ranges of significant correlation ($\alpha \leq 0.05$) are shown with red lines. The contribution of El Niño (*N*) is shaded in purple and the contribution from global ocean warmth (*O*) is shaded in yellow. The two have an overlapping area indicating the portion of positive collinearity. No colour is given to the portion of negative collinearity. Green vertical lines indicate the variability direction of *O* and $-O$.

components. Here, $-W$ and $-C$ point to cold-year La Niña and warm-year La Niña inversely. Note that 'warm' and 'cold' refer to global mean SST rather than the El Niño phenomenon itself. Figure 1 demonstrates how the two orthogonal spaces, one defined by TC climate and the other by the TC environment, are placed in a three-dimensional variability space. Projection of the TC climate framework onto the environmental framework points to the best explanatory environmental variability for each TC climate variability direction (Supplementary Fig. 4). A projection length (correlation) shows how much the TC climate variability is explained. The contribution of El Niño and global ocean warmth to the projection length is also identified.

Figure 2 presents the projection results for the global and six regional TC climates. The past 29-year (1984–2012) observations are used here on annual basis. Each indicator is the proxy of the synthetic environmental structure and is circularly chained. *A* and *E* have fixed positions as they are orthogonal to each other by definition, whereas *F* and *I* positions vary depending on TC climate (Supplementary Fig. 2). The best explanatory environment for each TC climate is marked in the upper abscissa. The response of western North Pacific TCs to the defined environment (both El Niño and global warming) is noticeably high and significant ($\alpha \leq 0.05$) at all directions (red line). Significant response in the eastern North Pacific and the North Atlantic occurs in a selective variability range. TCs in the North Indian region and the Southern Hemisphere are not well explained by this framework. This is not due to lower statistical power as the number of TCs is not the sample size. Each basin has 29 annual values. Nonetheless, the global TC climate coming from these regional features is seen to have a significant relationship with the defined environment at all directions.

It is found that El Niño is the best explanatory variability for global TC activity. On the other hand, global ocean warmth is the best explanatory variability for the efficiency of intensity, as indicated by the vertical green lines in Fig. 2. By construction, the efficiency of intensity is the intensity variation with activity variation removed. This result implies that global ocean warmth increases global TC intensity, but decreases frequency at the same time. Hence, the efficiency level explained by global ocean warmth is the amount (magnitude) of trade-off between intensity and frequency. Regionally the western North Pacific TC climate variability is similar to that of the globe as a whole. There is no direct link between the two, as regional values of intensity, activity and efficiency are determined by the regional frequency.

What physical mechanisms create the significant correlation between efficiency of intensification and ocean warming (large yellow area above E)? We pay special attention to the moisture increases in the tropics (30° S–30° N). By the Clausius–Clapeyron relationship, more moisture is evaporated from a warmer ocean surface, resulting in water vapour concentrating in the lower troposphere[11]. Figure 3a is a correlation map showing the vertical structure of moist static energy change by different environmental variability directions. Compared with other large-scale environmental changes, global ocean warming is clearly seen to be accompanied by a convectively more unstable troposphere. Moist air pumped from the lower troposphere moves upwards along the moist adiabat by which the upper air is heated[12].

In contrast to this warm anomaly prevailing in the middle and the upper troposphere in the tropics, moisture itself in the lower troposphere is not effectively transported out to the free atmosphere[11,13] (Supplementary Fig. 10). The consequences are warmer and drier conditions aloft, which is well reflected in the high-pressure anomaly over the middle and the upper troposphere (Fig. 3b). With the smaller Coriolis effect at lower latitudes, the high-pressure anomaly is well stratified and dominant over the tropics. Thus the two collinear environments, which are induced by the lower tropospheric moisture increase in association with the warmer global ocean, can be characterized as a more unstable troposphere but stronger high pressure in the middle and the upper troposphere. The high-pressure anomaly concentrates convection in time and space. These thermodynamic conditions over the global tropical cyclone activity imply fewer TCs, but efficient intensification once a TC is spawned to maintain a constant activity level. Thus TC intensity increases at the expense of TC frequency. In addition, a dynamic factor is examined using Hadley circulation strength (HCS). HCS is defined as the average of the maximum absolute mass streamfunction in each hemisphere. Its connection

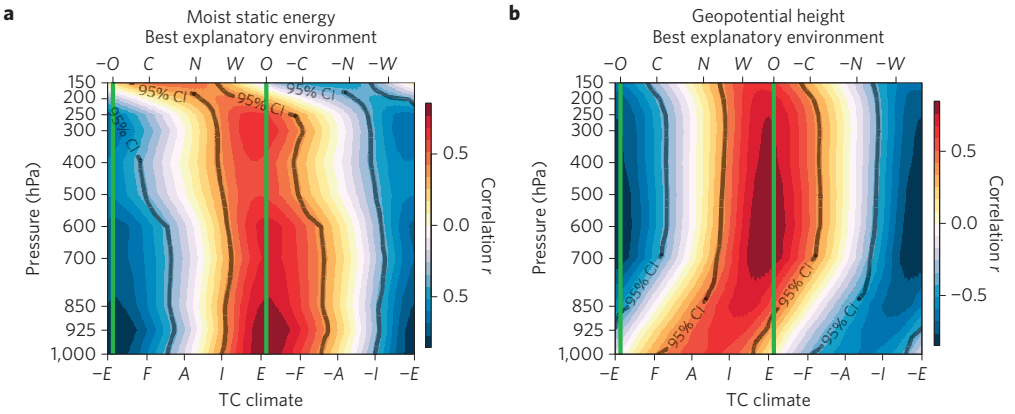


**Figure 3 | Correlation profiles. a**, Plotted for moist static energy. **b**, Plotted for geopotential height. Correlations are calculated with each environmental variability (upper abscissa) in the tropics (30° S–30° N). TC climate variability which can be best explained by each environmental variability is noted in the lower abscissa. Green vertical lines indicate the variability direction of *O* and *−O*.

with the global ocean warmth, however, seems insignificant, at least over the period studied here (Supplementary Fig. 11). This study is expected to provide a good basis for further understanding the mass flux response to global warming, which has been mostly examined by numerical models.

Observations indicate that global mean SST has increased by 0.30 °C over the past 30 years on average (Supplementary Fig. 9). Figure 4 shows how the increased global ocean warmth has influenced the magnitude of the trade-off between the intensity and the frequency of global TCs. Here, $\sigma$ is the standard deviation of global intensity and frequency simultaneously, which suggests a trade-off of 0.21 m s$^{-1}$ per TC (Supplementary Fig. 12). Inversely, the rate results in 4.7 fewer TCs per metre per second increase in average intensity. The efficiency of intensity can be estimated on this $\sigma$ level to estimate the amount of trade-off. The efficiency of intensity has increased by 0.74 $\sigma$ owing to the global mean SST increase. In physical units the trade-off amounts to 1.3 m s$^{-1}$ at the expense of 6.1 TCs over the period.

In spite of the regionally strong response of the efficiency of intensity in the western North Pacific (see Fig. 2) to warming seas, the contribution of this region to the global result is small. This is because the intensity level in this basin is higher, so a reduction in frequency implies a smaller contribution to the global intensity–frequency trade-off (Supplementary Fig. 5). Interestingly, the contribution in the North Atlantic is impressive. Despite the fact that the regional change of the efficiency of intensity is negative with global ocean warming (see Fig. 2), the contribution of this region to the global is positive and dominant. From the framework of statistical physics, the regional changes associated with global ocean warmth fix the global trade-off between intensity and frequency.

This study clarifies the connection between global TC climate and global warming. Instead of trend analysis, annual global mean SST is used to directly examine annual variations. This approach avoids the data quality problem occurring in a trend analysis when the observation technique advances over time[14]. A continuous variability space is applied that provides a broader and deeper understanding of the relationships not accessible from a restricted focus on frequency and intensity alone.

Results show that global ocean warmth best explains the variability direction associated with the efficiency of intensity. Subsequently, global ocean warmth is confirmed to bring about a convectively more unstable environment with more moisture in the lower troposphere, but a stronger high pressure aloft. This inhibits TC occurrences but provokes bursting intensities. Through the process, global warming over the ocean is seen to contribute to the efficiency of intensity. Intensity increases at the expense of frequency; hence, no change in overall activity. These results have important implications for the theory of climate. The methodology can be applied to TCs generated by dynamical climate models to better understand the meaning of TC climatology in future scenarios.

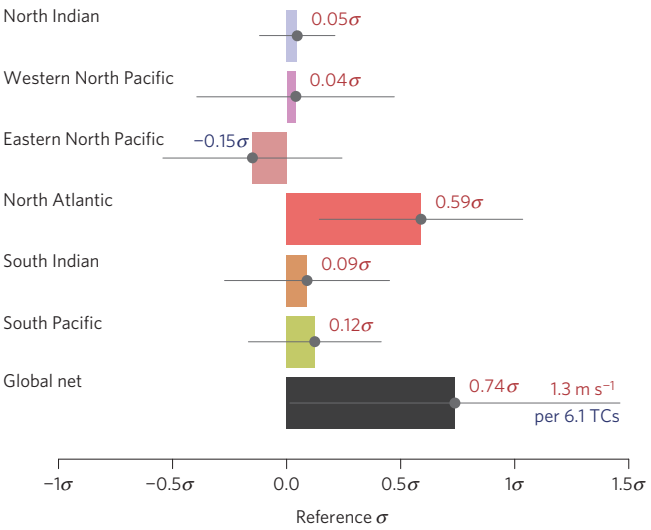


**Figure 4 | Influence of global ocean warming on the trade-off between intensity and frequency of global tropical cyclones.** 95% confidence intervals are shown in grey lines. Reference $\sigma$ is the standard deviation of global intensity and frequency at the same time. Regional contributions are shown with different colours. Red and blue characters represent positive and negative changes, respectively. Global trade-off amount is seen to have increased by 0.74$\sigma$ over the past 30 years, which is comparable to 1.3 m s$^{-1}$ increase of intensity at the expense of 6.1 TCs.

## Methods

Methods and any associated references are available in the online version of the paper.

Received 16 May 2014; accepted 2 April 2015;
published online 18 May 2015

## References

1. Webster, P. J., Holland, G. J., Curry, J. A. & Chang, H-R. Changes in tropical cyclone number, duration, and intensity in a warming environment. *Science* **309,** 1844–1846 (2005).

2. Bell, G. D. *et al.* Climate assessment for 1999. *Bull. Am. Meteorol. Soc.* **81,** s1–s50 (2000).
3. Emanuel, K. E. Increasing destructiveness of tropical cyclones over the past 30 years. *Nature* **436,** 686–688 (2005).
4. *Natural Hazards, Unnatural Disasters: The Economics of Effective Prevention* (World Bank, United Nations, 2010).
5. Mendelsohn, R., Emanuel, K., Chonabayashi, S. & Bakkensen, L. The impact of climate change on global tropical cyclone damage. *Nature Clim. Change* **2,** 205–209 (2012).
6. Knutson, T. R. *et al.* Tropical cyclones and climate change. *Nature Geosci.* **3,** 157–163 (2010).
7. Christensen, J. H. *et al.* in *Climate Change 2013: The Physical Science Basis* (eds Stocker, T. F. *et al.*) Ch. 14, 1248–1251 (IPCC, Cambridge Univ. Press, 2013).
8. Elsner, J. B., Kossin, J. P. & Jagger, T. H. The increasing intensity of the strongest tropical cyclones. *Nature* **455,** 92–95 (2008).
9. Holland, G. & Bruyère, C. Recent intense hurricane response to global climate change. *Clim. Dynam.* **42,** 617–627 (2014).
10. Kang, N-Y. & Elsner, J. B. An empirical framework for tropical cyclone climatology. *Clim. Dynam.* **39,** 669–680 (2012).
11. Vecchi, G. A. *et al.* Weakening of tropical Pacific atmospheric circulation due to anthropogenic forcing. *Nature* **441,** 73–76 (2006).
12. Chou, C., Wu, T-C. & Tan, P-H. Changes in gross moist stability in the tropics under global warming. *Clim. Dynam.* **41,** 2481–2496 (2013).
13. Held, I. M. & Soden, B. J. Robust responses of the hydrological cycle to global warming. *J. Clim.* **19,** 5686–5699 (2006).
14. Kossin, J. P., Olander, T. L. & Knapp, K. R. Trend analysis with a new global record of tropical cyclone intensity. *J. Clim.* **26,** 9960–9976 (2013).

## Acknowledgements

This research was supported by the Geophysical Fluid Dynamics Institute at the Florida State University (contribution number 471).

## Author contributions

Authors contributed equally to planning, experiment, analysis and writing, with N-Y.K. being the lead author.

## Additional information

Supplementary information is available in the online version of the paper. Reprints and permissions information is available online at www.nature.com/reprints. Correspondence and requests for materials should be addressed to N-Y.K.

## Competing financial interests

The authors declare no competing financial interests.

## Methods

Environmental variables come from the National Oceanic and Atmospheric Administration (NOAA) National Centers for Environmental Prediction (NCEP) reanalysis (http://www.esrl.noaa.gov/psd/data/gridded). To avoid the wind-conversion problem[15,16], global TC data set is organized by 1-min wind observations from the Joint Typhoon Warning Center (JTWC, http://www.usno.navy.mil/NOOC/nmfc-ph/RSS/jtwc/best_tracks) and the NOAA National Hurricane Center (NHC, http://www.nhc.noaa.gov/data). For the study, 29-year observations (1984–2012) are used. 1984 is the year when enhanced infrared (IR) satellite image analysis was developed[17,18], and also the year when the Japan Meteorological Agency (JMA) employed the objective Dvorak's satellite image analysis technique[19] to the operation procedure (see http://www.wmo.int/pages/prog/www/tcp/documents/JMAoperationalTCanalysis.pdf), which is thought to have improved the climate consensus between JTWC and JMA observations[20]. Considering the large number of western North Pacific TCs, the period of this study is also expected to increase the reliability of the global result. Statistics and figures are created using the software R (http://www.r-project.org) and are available from http://rpubs.com/Namyoung/P2014a.

## References

15. Song, J-J., Wang, Y. & Wu, L. Trend discrepancies among three best track data sets of western North Pacific tropical cyclones. *J. Geophys. Res.* **115,** D12128 (2010).
16. Knapp, K. R. & Kruk, M. C. Quantifying interagency differences in tropical cyclone best-track wind speed estimates. *Mon. Weath. Rev.* **38,** 1459–1473 (2010).
17. Dvorak, V. F. *Applications Laboratory Training Notes* (NOAA National Environmental Satellite Service, 1982).
18. Velden, C. *et al.* The Dvorak tropical cyclone intensity estimation technique: A satellite-based method that has endured for over 30 years. *Bull. Am. Meterol. Soc.* **87,** 1195–1210 (2006).
19. Dvorak, V. F. *Tropical Cyclone Intensity Analysis Using Satellite Data* Report no. 11 (NOAA Tech. Rep., 1984).
20. Kang, N-Y. & Elsner, J. B. Consensus on climate trends in western North Pacific tropical cyclones. *J. Clim.* **25,** 7564–7573 (2012).